Draft version April 2, 2018
Preprint typeset using LaTeX style emulateapj v. 08/22/09

CONSTRAINTS ON THE HIGH-ℓ POWER SPECTRUM OF MILLIMETER-WAVE ANISOTROPIES FROM APEX-SZ

C. L. Reichardt[1], O. Zahn[1], P. A. R. Ade[2], K. Basu[3], A. N. Bender[4], F. Bertoldi[5], H.-M. Cho[6], G. Chon[3,5,12], M. Dobbs[7], D. Ferrusca[1], N. W. Halverson[4,13], W. L. Holzapfel[1], C. Horellou[8], D. Johansson[8], B. R. Johnson[1], J. Kennedy[7], R. Kneissl[3,9,10], T. Lanting[2], A. T. Lee[1,11], M. Lueker[1], J. Mehl[14], K. M. Menten[3], M. Nord[3,5], F. Pacaud[5], P. L. Richards[1], R. Schaaf[5], D. Schwan[1], H. Spieler[11], A. Weiss[3], B. Westbrook[1]

Draft version April 2, 2018

ABSTRACT

We present measurements of the angular power spectrum of millimeter wave anisotropies with the APEX-SZ instrument. APEX-SZ has mapped 0.8 square degrees of sky at a frequency of 150 GHz with an angular resolution of 1′. These new measurements significantly improve the constraints on anisotropy power at 150 GHz over the range of angular multipoles $3000 < \ell < 10,000$, limiting the total astronomical signal in a flat band power to be less than 105 μK^2 at 95% CL. We expect both submillimeter-bright, dusty galaxies and to a lesser extent secondary CMB anisotropies from the Sunyaev-Zel'dovich effect (SZE) to significantly contribute to the observed power. Subtracting the SZE power spectrum expected for $\sigma_8 = 0.8$ and masking bright sources, the best fit value for the remaining power is $C_\ell = 1.1^{+0.9}_{-0.8} \times 10^{-5}$ μK^2 ($1.7^{+1.4}_{-1.3}$ Jy^2 sr^{-1}). This agrees well with model predictions for power due to submillimeter-bright, dusty galaxies. Comparing this power to the power detected by BLAST at 600 GHz, we find the frequency dependence of the source fluxes to be $S_\nu \propto \nu^{2.6^{+0.4}_{-0.2}}$ if both experiments measure the same population of sources. Simultaneously fitting for the amplitude of the SZE power spectrum and a Poisson distributed point source population, we place an upper limit on the matter fluctuation amplitude of $\sigma_8 < 1.18$ at 95% confidence.

Subject headings: cosmic microwave background — cosmology:observations — cosmology: cosmological parameters — infrared: galaxies

1. INTRODUCTION

Primary anisotropy in the cosmic microwave background (CMB) radiation is produced by inhomogeneities in the hot baryon-photon plasma at the epoch of recombination. The amplitude of these anisotropies as a function of angular scale has been used to infer precise constraints on the parameters of the standard ΛCDM model (Dunkley et al. 2009; Komatsu et al. 2009). On angular scales below several arcminutes, the primary anisotropy is damped by photon diffusion and the observed power is expected to be dominated by sources of foreground emission and the interaction of the CMB with intervening structure. In particular, the inverse Compton scattering of CMB photons off hot plasma bound to clusters of galaxies (Sunyaev & Zel'dovich 1972) gives rise to a spectral distortion of the CMB known as the Sunyaev-Zel'dovich effect (SZE). At frequencies less than ~ 220 GHz, the SZE produces a decrement in the CMB intensity in the direction of a galaxy cluster. Galaxy clusters produce (secondary) anisotropy power on arcminute scales corresponding to their angular size. The observed SZE power depends sensitively on the abundance of clusters and the history of structure formation. In particular, the amplitude of the SZE power scales as σ_8^7, where σ_8 is the rms fluctuation of matter on scales of $8\mathrm{h}^{-1}$ Mpc, and serves as an independent probe of the amplitude of density perturbations (Komatsu & Seljak 2002).

Evidence for small scale power beyond that expected from the primary CMB has been reported by the Berkeley Illinois Maryland Association (BIMA) and Cosmic Background Imager (CBI) interferometers operating at 30 GHz. These measurements find a level of SZE anisotropy power consistent with a value of σ_8 somewhat greater than those preferred by other contemporary measurements, which favor $\sigma_8 \sim 0.8$ (Vikhlinin et al. 2009; Komatsu et al. 2009). BIMA observations at 30 GHz covering a total of 0.1 deg^2 of sky produced a nearly 2σ detection of excess power in a flat band centered at a multipole $\ell = 5237$ (Dawson et al. 2006). Due to the non-Gaussian distribution of the SZE on the sky and the low significance of the detection, this resulted in only weak constraints on the matter power spectrum normal-

[1] Department of Physics, University of California, Berkeley, CA, 94720
[2] School of Physics and Astronomy, Cardiff University, CF24 3YB Wales, UK
[3] Max Planck Institute for Radioastronomy, 53121 Bonn, Germany
[4] Center for Astrophysics and Space Astronomy, Department of Astrophysical and Planetary Sciences, University of Colorado, Boulder, CO 80309
[5] Argelander Institute for Astronomy, Bonn University, Bonn, Germany
[6] National Institute of Standards and Technology, Boulder, CO, 80305
[7] Department of Physics, McGill University, Montréal, Canada, H3A 2T8
[8] Onsala Space Observatory, Chalmers University of Technology, SE-439 92 Onsala, Sweden
[9] Joint ALMA Office, Av El Golf 40, Piso 18, Santiago, Chile
[10] ESO, Alonso de Cordova 3107, Vitacura, Santiago, Chile
[11] Lawrence Berkeley National Laboratory, Berkeley, CA, 94720
[12] Max Planck Institute for Extraterrestrial Physics, 85748 Garching, Germany
[13] Department of Physics, University of Colorado, Boulder, CO 80309
[14] University of Chicago, 5640 South Ellis Avenue, Chicago, IL 60637

ization, $\sigma_8 = 1.03^{+0.20}_{-0.29}$ at 68% confidence. Observations with the CBI experiment at 30 GHz over a larger field were used to produce a $> 3\sigma$ detection of excess power on angular scales $\ell \in [1800, 4000]$ (Sievers et al. 2009). Interpreting this power as being due to the SZE, they find $\sigma_8 = 1.015 \pm 0.06$ at 68% confidence. However, recent observations with the SZA experiment operating at 30 GHz and covering a total of 2 deg^2 of sky, have determined an upper limit on the excess power in broad band centered at multipole $\ell = 4066$ which is significantly lower than the band powers reported by CBI and appears to be consistent with more conventional values of $\sigma_8 \sim 0.8$ (Sharp et al. 2009). The SZA team interprets the higher power measured by CBI as potentially being due to an unsubtracted population of radio sources.

At 150 GHz, we expect the SZE and emission from distant dusty galaxies to contribute significantly to the power on angular scales corresponding to $\ell > 2500$. The ACBAR experiment reported a $\sim 1\sigma$ excess power at $\ell > 2000$, that if interpreted as the SZE, would be consistent with the higher value for σ_8 preferred by CBI (Reichardt et al. 2009). However, the ACBAR results are in excellent agreement with a more standard value $\sigma_8 \sim 0.8$ when one considers the expected foreground emission from IR point sources. The QUaD collaboration has recently released a 150 GHz power spectrum for $\ell > 2000$ (QUaD collaboration: R. B. Friedman et al. 2009). The QUaD bandpowers appear (numerical values have not yet been released) to be systematically lower than those produced by ACBAR with no evidence for contributions from secondary anisotropy or foreground emission. Bolocam has recently published new results for anisotropy power at 150 GHz on angular scales above $\ell = 3000$ (Sayers et al. 2009). They report upper limits on the power of $1080\,\mu\mathrm{K}^2$ at 95% confidence in a wide bin centered at $\ell = 5700$ and determine that $\sigma_8 < 1.57$ at 90% confidence. New high resolution and sensitivity bolometer arrays operating at millimeter wavelengths such as those currently deployed on the APEX, SPT, and ACT telescopes have the capacity to drastically improve constraints on the SZE and point source contributions to the high-ℓ power spectrum.

This paper presents new measurements of small scale anisotropy power made with the APEX-SZ bolometer array on the Atacama Pathfinder Experiment (APEX) telescope from its high elevation site in the Atacama Desert. This work significantly improves the constraints on excess power above that expected from primary CMB anisotropy at $\ell > 3000$ at a frequency of 150 GHz. In Section 2, we describe the APEX-SZ instrument and the observations used to produce the results presented in this paper. The beam and calibration of the instrument are described in Section 3. The algorithms used in the production of the temperature maps and the power spectrum are described in Section 4. In Section 5, we present the power spectrum results and address sources of foreground emission. Our conclusions are summarized in Section 6.

2. INSTRUMENT AND OBSERVATIONS

APEX-SZ is an array of 330 transition-edge superconducting (TES) bolometers operating at 150 GHz (Schwan et al. 2003; Dobbs et al. 2006; Schwan et al. 2009). The bolometers are cooled to 280 mK via a three stage He sorption fridge and mechanical pulse tube cooler and instrumented with a frequency-domain multiplexed readout system. The array observes from the 12m APEX telescope on the Atacama plateau in Chile (Güsten et al. 2006) and has approximately $1'$ FWHM beams with a $22'$ field-of-view (FOV). The extremely dry and stable atmospheric conditions make the Atacama one of the best sites for millimeter-wave astronomy.

The band powers reported in this work are derived from a single, 0.8 deg^2 field observed by APEX-SZ for 10 nights in August and September of 2007. This field is a subset of the XMM-LSS field (Pierre et al. 2004) and is centered on a moderately massive, X-ray detected cluster, XLSSU J022145.2-034614, with an X-ray temperature of 5 keV (Willis et al. 2005; Pacaud et al. 2007). A joint analysis of the X-ray and SZ data will be undertaken in a separate paper. A circular scan strategy was used instead of a raster scan to improve the observing efficiency. The scan strategy concentrates the integration time at the center of the map causing the time per pixel to increase steadily from the edges of the map to the center. The total integration time is 2.9k detector-hours. The map center reached a depth of 12 μK per $1'$ pixel. More details on the instrument and scan strategy can be found in Halverson et al. (2009) (hereafter H08) and Schwan et al. (2009).

3. BEAM AND CALIBRATION

The average beam of the APEX-SZ bolometers is measured with daily observations of Mars. At $8''$ diameter, Mars is nearly a point source for the $1'$ APEX-SZ beam, and it is sufficiently bright to map the beam near sidelobes to below -25 dB. The measured beam agrees well with the ZEMAX[15] simulated beam profiles when optical cross-talk is taken into account. The near sidelobes increase the real beam solid angle by 32% compared to the best fit Gaussian beam. We divide the measurement uncertainty on the beam into two parts. The main lobe is well-fit by a Gaussian, and we estimate the measurement uncertainty on the FWHM to be 2.5%. Due to the large angular scale of the sidelobe structure, a mis-estimation of beam sidelobe will effectively cause a mis-calibration of the band powers. We include the uncertainty in the total beam area in the calibration error.

The observations of Mars are used to establish the absolute calibration of the APEX-SZ instrument. The temperature of Mars for our observation frequency and dates is taken from the Rudy model (Rudy et al. 1987; Muhleman & Berge 1991), that has been updated and maintained by Bryan Butler[16]. The Rudy model is compared with measurements of the brightness temperature of Mars made with the WMAP satellite at 93 GHz during five periods across several years (Hill et al. 2009). The WMAP measurements of Mars have uncertainty of $< 1\%$ and we adjust the normalization of the Rudy Model down by 5.2% to bring it into agreement with the WMAP measurements. Combining the $\sim 1\%$ uncertainty in the WMAP Mars measurements, the 1.0% scatter in the 93 GHz WMAP to Rudy Model comparison, and 0.9% for the uncertainty in the extrapolation from 93 GHz, where the Rudy Model is calibrated, to our observing frequency, we find the total uncertainty in the

[15] http://www.zemax.com
[16] http://www.aoc.nrao.edu/∼bbutler/work/mars/model/

Mars brightness temperature to be 1.7%.

The calibration of each detector is set by comparing the peak amplitude in a map of Mars to the expected amplitude given the temperature and size of Mars and the size of the detector's beam. A correction factor for the atmospheric opacity is applied which is always less than 3%. The overall calibration uncertainty is estimated to be 5.5% in temperature, with the dominant errors due to a 4% uncertainty in the beam area, a 3% uncertainty to account for temporal variations between the model prediction and the temperature measured by APEX-SZ, the 1.7% uncertainty in the temperature of Mars, and a 1.4% uncertainty in the conversion of brightness temperature to CMB temperature for the measured APEX-SZ band. More details on the beam estimation and calibration can be found in H08.

4. ANALYSIS

4.1. *Map-Making*

The filtering and map-making process used in this analysis follows the approach detailed in H08 for analysis of the Bullet cluster. We briefly outline the major steps here, while highlighting any differences in the filtering between this work and the Bullet cluster analysis. The timestream processing is designed to remove scan-synchronous noise, atmospheric fluctuations, and 1/f noise. The scan pattern includes boresight elevation changes which modulate the air mass along the line of sight. This signal is removed by fitting for a cosecant(el) term. 1/f noise in the system is filtered from the timestream by a 0.3 Hz 8-pole Butterworth high-pass filter (HPF). The typical length scale of atmospheric fluctuations is much larger than the FOV, so fluctuations are highly correlated across the APEX-SZ array. This correlated term is removed by fitting for a low order spatial polynomial across the focal plane at each time sample. We remove a 2^{nd} order spatial mode in this work. The cumulative effect of the filtering is to completely remove structures corresponding to angular multipoles below $\ell \simeq 1400$. After filtering, the timestreams are weighted according to the filtered timestream RMS and binned into $20''$ map pixels.

4.2. *Power Spectrum Estimation*

The band powers, q_B, are reported in CMB temperature units of μK^2 and parametrize the power spectrum according to

$$\frac{\ell(\ell+1)}{2\pi} C_\ell \equiv D_\ell = \sum_B q_B \chi_{B\ell} \tag{1}$$

where $\chi_{B\ell}$ are top hat functions; $\chi_{B\ell} = 1$ for $\ell \in B$ and 0 for $\ell \notin B$. We use a pseudo-C_ℓ power spectrum estimator (Hivon et al. 2002). In this formalism, the map spectrum (also called the pseudo-C_ℓ or $\tilde{C}_\ell$) depends on the true spectrum (C_ℓ) as:

$$\tilde{C}_\ell = M_{\ell\ell'} T_{\ell'} B^2_{\ell'} C_{\ell'}. \tag{2}$$

$\tilde{C}_\ell$ is calculated using the flat-sky approximation, in which the spherical harmonic transform of the sky reduces to a Fourier transform of the map. This is an excellent approximation for a sub-degree sized map. The experimental beam function is described by B_ℓ, and the mode-coupling due to finite sky coverage is denoted by $M_{\ell\ell'}$. T_ℓ represents the transfer function of the map-making process which would ideally be equal to one. In practice, the HPF applied to the APEX-SZ timestreams eliminates power on scales $\ell < 1400$ so $T_\ell = 0$ on these scales and remains below one at all ℓ. Following the MASTER algorithm (Hivon et al. 2002), we measure the transfer function using a set of Monte-Carlo sky realizations that have been passed through the full pipeline, from the timestreams to the maps. These simulated sky maps include a lensed WMAP5+ACBAR best fit CMB model (Hill et al. 2009; Reichardt et al. 2009), realizations of the SZE signal (Shaw et al. 2009), and realizations of the point source populations (Negrello et al. 2007; Granato et al. 2004; de Zotti et al. 2005). This set of signal-only simulations is also used to estimate the cosmic variance contribution to the band power uncertainties.

The mode-coupling matrix $M_{\ell\ell'}$ is calculated analytically for the two sky masks used to estimate the APEX-SZ band powers. These masks describe the weighting applied to each pixel in the map before calculating the Fourier transform and are analogous to windowing data in a 1D Fourier transform. We begin by applying an inverse-noise weighting to each pixel, based on the diagonal elements of the pixel-pixel noise covariance matrix. This effectively de-weights the noisy edges of the map, and is near-optimal in the low signal-to-noise per pixel regime. We modify this simple mask to exclude pixels near detected clusters or point sources. There are two X-ray detected clusters in the field; XLSSU J022145.2-034614 and XLSSU J022157.4-034001. The field was centered on the first and more massive of these clusters, which would introduce a bias into the determination of the SZE amplitude. The central cluster is masked to a diameter of $6'$ in the first mask, hereafter the *Cluster* mask. The second cluster is fainter, and was detected only in a joint analysis of X-ray and optical data (Andreon et al. 2005). We tested the effects of masking the second cluster as well and did not see a significant change in the band powers. The second mask removes the 27 point sources detected in the APEX-SZ map in addition to the central cluster. These sources are found by using SExtractor (Bertin & Arnouts 1996) to select sets of neighboring pixels above $3\,\sigma$ in an optimally filtered map. This corresponds approximately to a detection threshold of 2 mJy. We discuss these sources further in §5.1. This mask will be referred to as the *Cluster + Sources* mask. We tested the effect of masking all NVSS or bright Spitzer sources within the field, and observed no significant change in power.

The measured band powers will be the sum of the signal and noise band powers,

$$D_\ell = D^S_\ell + D^N_\ell \tag{3}$$

and we must subtract the expected noise contribution to recover the underlying signal spectrum. The noise contribution to the APEX-SZ band powers is estimated from the average power in a set of 2200 jack-knife maps between two randomly selected half sets of the ∼1100 complete observations of the field. These difference maps effectively remove sky signal, while preserving correlated noise in the timestreams on time scales shorter than

the few minute length of a scan with randomized phase. Noise on longer time scales has been removed by the 0.3 Hz HPF. The expectation value of the noise band powers, $\langle D_\ell^N \rangle$, is taken to be the mean band powers measured across the set of 2200 jack-knives. The approach is similar to that used in the analysis of the Bolocam power spectrum (Sayers et al. 2009). We apply the same procedure to signal-only simulated maps and confirm that any residual signal power due to the small pointing, filtering and weighting differences between observations is negligible.

5. BAND POWERS AND σ_8

The power spectrum presented in Figure 1 is the product of applying the analysis in Section 4 to APEX-SZ observations of the XMM-LSS field. The band powers for angular multipoles from 3000 to 10,000 are tabulated in Table 1. The band powers can be compared to a theoretical model using the window functions. The numerical values for the band powers and window functions can be downloaded from the APEX-SZ website[17].

The APEX-SZ band powers show a tendency to increase on smaller angular scales, suggestive of the ℓ^2 shape that a Poisson distribution of point sources will have in a plot of $\ell(\ell+1)C_\ell/2\pi$. The contribution of the primary CMB will be small at these small angular scales, and we subtract the estimated contribution for the best fit WMAP5+ACBAR lensed ΛCDM power spectrum before fitting for the amplitude of a constant C_ℓ. The beam and calibration uncertainty is incorporated by averaging the likelihood function over a set of 200 Monte Carlo realizations. The best fit power is $C_\ell = 1.0^{+0.9}_{-0.6} \times 10^{-5}\,\mu\mathrm{K}^2$, which includes both the point source and SZE contributions. Results for both masks are tabulated in the first row of Table 2. If the expected SZE power spectrum for $\sigma_8 = 0.8$ is subtracted in addition to the primary anisotropies, the average C_ℓ drops slightly to $0.9^{+0.9}_{-0.6} \times 10^{-5}\,\mu\mathrm{K}^2$. At the best-fit point source amplitude for $\sigma_8 = 0.8$, 92% of the astronomical power in the map is produced by point sources rather than the SZE. These results are obtained after masking the bright, central cluster. Leaving the central cluster unmasked increases the fit power by $\sim 1.0 \times 10^{-5}\,\mu\mathrm{K}^2$. We also report the results after masking the sources internally detected in the map at $> 3\sigma$ in the second row of Table 2. These results are consistent with and improved over the previous ACBAR constraints from $\ell < 3000$ of $C_\ell = 2.7^{+1.1}_{-2.6} \times 10^{-5}\,\mu\mathrm{K}^2$. However, these numbers should be compared with caution as the two experiments have different flux cuts for source masking, and the excess power will depend on the flux to which sources have been masked.

We also investigate the effects of allowing the amplitude of the SZE power spectrum to float freely. The SZE power spectrum template is based on the simulations in Shaw et al. (2009). The simulations are for a WMAP5 cosmology with $\sigma_8 = 0.77$. The amplitude of the SZE power spectrum is expected to scale approximately as σ_8^7, so the derived SZE amplitude can be related to σ_8. In practice, the APEX-SZ data set lacks the sensitivity to make a detection of SZE power; however, the results can be used to place an upper limit on σ_8. The upper limits on σ_8 and the point source amplitudes for the joint fit are reported in Table 2. We assume a flat prior on σ_8. The exact amplitude of the SZE spectrum is only poorly understood, leading to a 10% systematic uncertainty on σ_8 (Komatsu & Seljak 2002). This systematic uncertainty is not included in the reported upper limits.

The non-Gaussian distribution of the SZE is very important on small patches of sky (Cooray 2001; Zhang et al. 2006). We incorporate the non-Gaussian statistics into our analysis by returning to the set of simulated SZ skys (Shaw et al. 2009). We extract 7500 independent realizations of the APEX-SZ map and calculate the power in each realization under the two masks. The maps have been convolved by the experimental beam and do not include noise. This process maps out the full, non-Gaussian cosmic variance of the expected SZE power for $\sigma_8 = 0.77$. We scale this to other cosmologies by assuming that the probability of measuring a power X will scale with σ_8 as

$$P(X|\sigma_8) = \left(\frac{\sigma_8}{0.77}\right)^7 P\left(\left(\frac{0.77}{\sigma_8}\right)^7 X\,|\sigma_8 = 0.77\right). \quad (4)$$

Bayes' theorem with a flat prior in σ_8 is applied to find a posterior probability density, $P(\sigma_8|X)$. We determine the probability of a given SZE power from the data by marginalizing over a point source component as described in the last paragraph. Finally, the likelihood function of σ_8 given the APEX-SZ data $\mathbf{d}$ is calculated by

$$P(\sigma_8|\mathbf{d}) = \int dX\, P(\sigma_8|X) P(X|\mathbf{d}) \quad (5)$$

and integrated to find the 95% CL upper limit on σ_8. The limit rises to $\sigma_8 < 1.18$, substantially weaker than the limit of $\sigma_8 < 0.94$ derived under Gaussian assumptions (see the third row of Table 2, labeled "Unconstrained σ_8"). The marginalized likelihood function for both σ_8 and C_ℓ^{PS} are plotted in Figure 2, while the 2d likelihood surface for both parameters is shown in Figure 3. The upper limit is sensitive to the prior chosen since APEX-SZ does not make a detection of SZE power. A flat prior on power, σ_8^7, strongly prefers higher values of σ_8 than the flat prior on σ_8, and raises the upper limit from 1.18 to $\sigma_8 < 1.50$ at 95% CL. This is entirely due to the weighting by the prior as the prior probability for $\sigma_8 = 2$ is 240 times the probability of $\sigma_8 = 0.8$.

Finally, we combine the four APEX-SZ band powers into a single band to facilitate the comparison to other data sets. The resulting upper limit is $\sim 100\,\mu\mathrm{K}^2$ after including the APEX-SZ calibration and beam uncertainty as shown in the last row of Table 2, "Flat Excess". We have assumed that D_ℓ is constant across the four bands and subtracted the contribution due to the primary CMB anisotropies. However, this upper limit does not include a non-Gaussian contribution to cosmic variance.

5.1. *Radio and IR source contributions*

Submillimeter bright galaxies and radio sources are expected to dominate the primary temperature anisotropies for $\ell \gtrsim 2500$ at 150 GHz. The exact contribution from point sources, especially radio sources, will

[17] http://bolo.berkeley.edu/apexsz/index.html

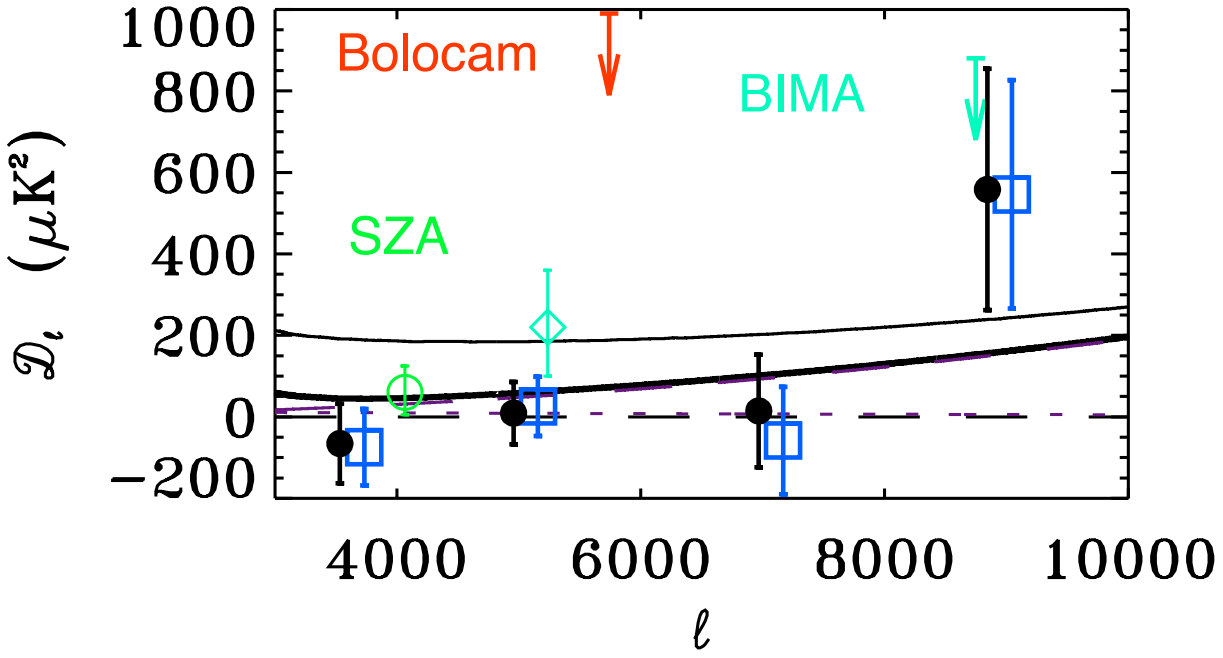

FIG. 1.— Band powers derived from the APEX-SZ map plotted over a model (**thick black line**) including the primary CMB anisotropies, a SZE model for $\sigma_8 = 0.8$ (**short dashed purple line**) , and the predicted point source contribution for a 2 mJy cut threshold (**long dashed purple line**) . This model is not a fit to the APEX-SZ band powers. We also plot for comparison the theory spectrum (**thin black line**) if we increase σ_8 to APEX-SZ's 95% CL upper limit of 1.18. The APEX-SZ band powers for the *Cluster* mask are plotted with **blue squares**, while the *Cluster+Sources* mask results are shown as **black circles**. The *Cluster* mask band powers have been shifted by $\Delta\ell = 200$ to the right for clarity. BIMA (**turquoise diamond and upper limit** - Dawson et al. (2006)), SZA (**green circle** - Sharp et al. (2009)), and Bolocam (**red upper limit** - Sayers et al. (2009)) have previously released band-powers centered at $\ell > 3000$. The upper limits are shown at 95% CL. BIMA and SZA operate at 30 GHz where there will be four times as much SZE power as at 150 GHz and we expect the foregrounds to be dominated by radio sources rather than dusty galaxies. The plotted theory spectra are for 150 GHz only.

TABLE 1
BAND POWERS

		Cluster masked		Cluster + Sources masked	
ℓ range	$\ell_{\rm eff}$	q (μK^2)	σ (μK^2)	q (μK^2)	σ (μK^2)
3000-4000	3532	-74	94	-66	98
4000-6000	4957	26	73	9	77
6000-8000	6968	-58	132	14	138
8000-10000	8844	546	280	558	296

NOTE. — Band multipole range and weighted value $\ell_{\rm eff}$, band powers q, and uncertainty σ from the analysis of the XMM-LSS field with two masks. The first two columns (*Cluster masked*) show the results when the central X-ray detected cluster in the field is masked to 6′ diameter. The second set of columns (*Cluster + Sources masked*) masks twenty-seven $> 3\sigma$ sources detected in the map to 1.5′ diameter as well as the cluster. More details on the masks can be found in §4.2.

depend on our ability to detect and mask the brightest sources. The exact $3\,\sigma$ detection threshold in the APEX-SZ map depends on the map position due to the uneven coverage, but is approximately 2 mJy on average. As discussed below, the predicted band powers are fairly insensitive to the precise cut level unless it shifts by an order of magnitude. We assume both populations are drawn from a Poisson distribution.

The number counts of dusty, submillimeter bright galaxies are modeled in Negrello et al. (2007) based on surveys at higher frequencies. Deep, high-resolution maps of the 150 GHz sky are expected to be confusion-limited by these sources. The anisotropies are the result of variations in the number of very faint sources with fluxes around 0.5 mJy. A 1 mJy point source will produce an increment of 20 μK in the APEX-SZ map. The APEX-SZ map of the XMM-LSS field is too shallow to pick out these sub-mJy sources, and we see no evidence of reaching the confusion-limit in the current observations. The dusty galaxy contribution to the APEX-SZ band powers is predicted by the model presented in Negrello et al. (2007) to be $C_\ell = 1.1 \times 10^{-5}$ μK^2 (1.7 Jy^2 sr^{-1}) in the absence of clustering, which is in good agreement with the measured point source power in Table 2. The predicted power from dusty galaxies is nearly independent of the flux cut level above 1 mJy. Dusty galaxies are expected to account for most of the power in the APEX-SZ maps.

The BLAST collaboration recently released measurements of the power spectrum of the cosmic far-infrared

TABLE 2
POINT SOURCE POWER AND σ_8 CONSTRAINTS

	Cluster masked	Cluster + Sources masked
Zero SZE power:		
C_ℓ^{PS} (10^{-5} μK^2)	$1.0^{+0.9}_{-0.6}$	$1.2^{+1.0}_{-0.8}$
Fixed $\sigma_8 = 0.8$:		
C_ℓ^{PS} (10^{-5} μK^2)	$0.9^{+0.9}_{-0.6}$	$1.1^{+0.9}_{-0.8}$
Unconstrained σ_8:		
C_ℓ^{PS} (10^{-5} μK^2)	$0.9^{+0.9}_{-0.6}$	$1.1^{+0.9}_{-0.8}$
σ_8 (G) (95% CL)	0.94	0.94
σ_8 (NG) (95% CL)	1.18	1.18
Flat excess:		
(with $\ell_{center} = 4966$)		
D_ℓ (μK^2)	33^{+37}_{-24}	36^{+39}_{-26}
95% CL	97	105

NOTE. — The constraint on point source power C_ℓ^{PS}, and the 95% CL upper limit on σ_8 derived from the APEX-SZ data set are tabulated for different assumptions about the SZE power and masks. The expected primary CMB anisotropy power has been subtracted from the measured band powers. We show the upper limit on σ_8 with (NG) and without (G) accounting for the non-Gaussian distribution of the SZE. Accounting for the non-Gaussianity in the expected SZE sky weakens the upper limit considerably. The first column (*Cluster masked*) shows the results when the massive, X-ray detected cluster in the field is masked to 6′ diameter. The second column (*Cluster + Sources masked*) excludes the $> 3\sigma$ sources detected in the map as well as the cluster. More details on the masks can be found in §4.2. The measured point source power is in excellent agreement with the predicted amplitude of 1.1×10^{-5} μK^2 (1.7 Jy^2 sr^{-1}) for the sum of the radio and dusty galaxy models in all cases. We also show the results under the assumption that the power at high-ℓ above the primary CMB anisotropies can be modeled as a flat band-power. The 95% CL upper limit on a flat excess of $<$105 μK^2 includes the beam and calibration uncertainties but does not include non-Gaussian contributions to cosmic variance.

background at frequencies of 600 GHz to 1.2 THz (Viero et al. 2009). BLAST measured a Poisson contribution from star-forming galaxies with an amplitude of $2.63 \pm 0.1 \times 10^3$ Jy^2 sr^{-1} at 600 GHz. A clustering term is detected as well on angular scales larger than those probed by APEX-SZ. Expressing the frequency dependence of the source fluxes as $S(\nu) \propto \nu^\alpha$, we can derive an effective spectral index, α, by comparing the power measured by BLAST at 600 GHz to the point source power likelihood function of the APEX-SZ maps at 150 GHz. This index will depend on the the spectra of the individual galaxies and their redshift distribution. We find that a spectral index of $\alpha = 2.64^{+0.4}_{-0.2}$ scales the BLAST power to match the best-fit $C_\ell = 1.1^{+0.9}_{-0.8} \times 10^{-5}$ μK^2 ($1.7^{+1.4}_{-1.3}$ Jy^2 sr^{-1}) of the APEX-SZ data. This inferred spectral index agrees well with previous estimates for sub-mm bright galaxies. Knox et al. (2004) examined nearby galaxy data and found $S_\nu \propto \nu^{2.6 \pm 0.3}$. In an alternative approach, Greve et al. (2004) compared the flux of sources in overlapping regions observed by MAMBO (1.2 mm) and SCUBA (850 μm) and found the fluxes scaled as $S_\nu \propto \nu^{2.65}$. The point source power in the APEX-SZ data set at 150 GHz is consistent with being entirely due to a population of dusty submm-bright galaxies such as those observed by BLAST.

We also consider radio sources as a potential foreground in the APEX-SZ maps. Granato et al. (2004) and de Zotti et al. (2005) have modeled the number counts of several classes of radio sources at tens of GHz. We derive $C_\ell^{\rm radio}$ from their modeled number counts at 150 GHz. The radio source power is dependent on the brightest objects and is expected to scale approximately linearly with the source cut threshold. At the 2 mJy source cut threshold of APEX-SZ, $C_\ell^{\rm radio}$ should be $\lesssim 5\%$ of the dusty galaxy contribution.

We find 27 point sources above 3 σ ($\sim$2 mJy) in the APEX-SZ maps using the approach outlined in §4.2. Eight of these sources are within 1′ of a NVSS source and are likely radio sources. We expect four false detections based on Gaussian statistics and the number of beam-sized pixels in the APEX-SZ map. The remaining sources are tentatively identified as dusty galaxies. We can compare the observed number counts in the APEX-SZ maps with other experiments at 150 GHz, however most previous experiments were targeting larger angular scales and are relatively insensitive to dim point sources. QUaD (QUaD collaboration: R. B. Friedman et al. 2009) and ACBAR (Reichardt et al. 2009) both report $\sim$0.1 radio sources per square degree with a flux detection threshold of many tens of mJy. The deepest previously published map at 150 GHz is from Bolocam (Sayers et al. 2009) which reports no sources above 10 mJy in a 1 deg^2 patch. As dN(>S)/dS is expected to fall steeply above 1 mJy for dusty galaxies, the scarcity of detected sources in these maps is not particularly surprising. The BLAST source catalogue (Dye et al. 2009) of 351 sources detected at 250, 350 or 500 μm allows a more interesting cross-comparison. The BLAST catalogue has 294 sources per square degree in the deep coverage region and 15 sources per square degree in the shallow coverage region. At 500 μm, the detection threshold of the BLAST catalogue is 30 mJy and 100 mJy respectively. For the best-fit effective spectral index of $\alpha = 2.64$ derived earlier, this corresponds to a source detection threshold at 150 GHz of 0.8 and 2.6 mJy respectively. These two detection thresholds bracket the average APEX-SZ 3 σ detection threshold of 2 mJy, and the observed APEX-SZ non-radio source

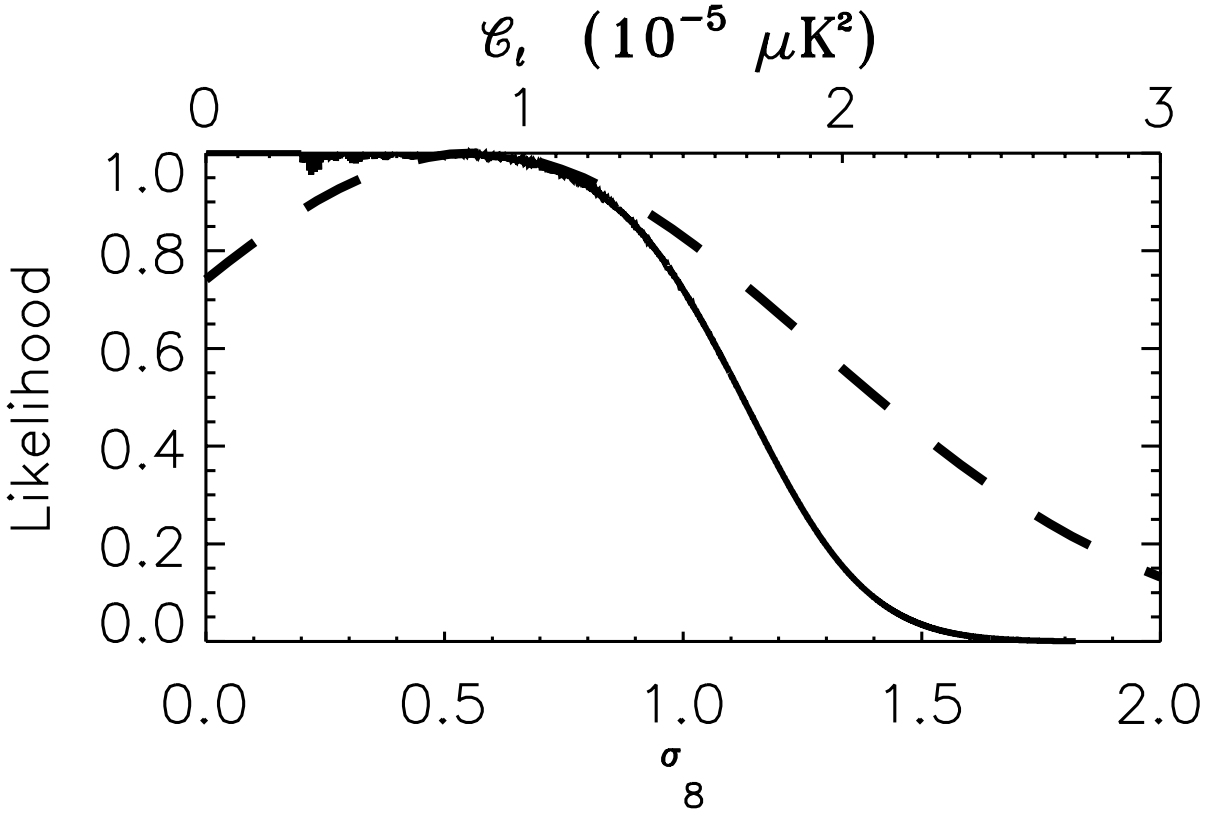

FIG. 2.— [*solid and lower x-axis*] Marginalized likelihood function for σ_8 for a flat prior on σ_8 after accounting for non-Gaussianity. [*dashed and upper x-axis*] Marginalized likelihood function for C_ℓ^{ps}. These curves are for the *Cluster+Sources* mask.

number density of 19 sources/deg^2 falls between these two source densities as we would expect. The source number counts in the APEX-SZ maps appear consistent with the numbers expected for dusty galaxies.

6. CONCLUSIONS

Observations with the APEX-SZ instrument have been used to constrain the power in excess of the primary CMB temperature anisotropies at 150 GHz. This power is expected to be dominated by emission from sub-mm bright, dusty galaxies and the APEX-SZ band powers are consistent with this hypothesis. We find excellent agreement between the point source power in the APEX-SZ maps and model predictions based on observations at other frequencies. We estimate that the flux of these sub-mm bright galaxies scales with frequency as $S_\nu \sim \nu^{2.64}$ by comparing the power measured by BLAST at 600 GHz to the best-fit point source power in the APEX-SZ maps at 150 GHz. Determining the contribution of these foreground sources not only constrains models for the population of dusty galaxies, but is important for planning current and future observations of secondary CMB anisotropies at these wavelengths.

We also place upper limits on σ_8 from fits to the amplitude of the SZE power spectrum while marginalizing over a Poisson point source contribution. We assume a template for the SZE power spectrum derived from simulations by Shaw et al. (2009) with the amplitude of the SZE power spectrum scaling as σ_8^7. We find an upper limit of $\sigma_8 < 1.18$ at 95% confidence. This result is similar to the constraints from the CBI and BIMA interferometers operating at 30 GHz. The limits from SZA, QUaD, or ACBAR would likely be slightly lower, but they did not express their results in terms of upper limits on σ_8. At these frequencies and angular scales, the previous best limit comes from Sayers et al. (2009), who used observations with the Bolocam instrument to constrain $\sigma_8 < 1.57$ at 90% confidence.

A third of the APEX-SZ instrument was recently upgraded to more sensitive detectors with improved optical efficiencies. In the next year, the remainder of the focal plane will be upgraded resulting in significant improvements to the instrument's mapping speed. The instrument will continue observing in the next several years with a focus on developing a catalog of clusters with SZE, X-ray and optical observations across the Southern hemisphere.

7. ACKNOWLEDGMENTS

We thank the staff at the APEX telescope site, led by David Rabanus and previously by Lars-Åke Nyman, for their dedicated and exceptional support. We also thank LBNL engineers John Joseph and Chinh Vu for their work on the readout electronics. APEX-SZ is funded by the National Science Foundation under Grant No. AST-0138348. Work at LBNL is supported by the Director, Office of Science, Office of High Energy and Nuclear Physics, of the U.S. Department of Energy under Contract No. DE-AC02-05CH11231. Work at McGill is supported by the Natural Sciences and Engineering Research Council of Canada and the Canadian Institute for Advanced Research. This research used resources of the

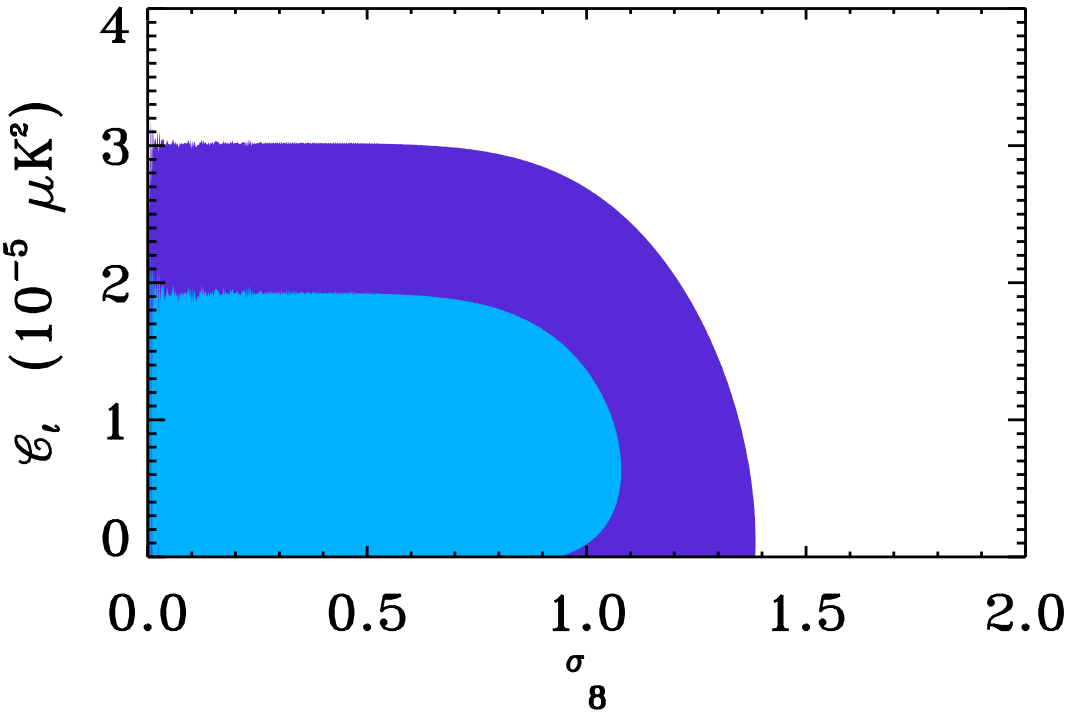

FIG. 3.— The 1-σ and 2-σ contours on the 2D likelihood surface for σ_8 and the point source amplitude for the *Cluster+Sources* mask applied to the APEX-SZ map. The contours include the effects of non-Gaussianity in the SZE. A flat prior on σ_8 has been assumed.

National Energy Research Scientific Computing Center, which is supported by the Office of Science of the U.S. Department of Energy under Contract No. DE-AC02-05CH11231. Nils Halverson acknowledges support from an Alfred P. Sloan Research Fellowship.

REFERENCES

Andreon, S., Valtchanov, I., Jones, L. R., Altieri, B., Bremer, M., Willis, J., Pierre, M., & Quintana, H. 2005, MNRAS, 359, 1250
Bertin, E. & Arnouts, S. 1996, A&AS, 117, 393
Cooray, A. 2001, Phys. Rev. D, 64, 063514
Dawson, K. S., Holzapfel, W. L., Carlstrom, J. E., Joy, M., & LaRoque, S. J. 2006, ApJ, 647, 13
de Zotti, G., Ricci, R., Mesa, D., Silva, L., Mazzotta, P., Toffolatti, L., & González-Nuevo, J. 2005, A&A, 431, 893
Dobbs, M., Halverson, N. W., Ade, P. A. R., Basu, K., Beelen, A., Bertoldi, F., Cohalan, C., Cho, H. M., Güsten, R., Holzapfel, W. L., Kermish, Z., Kneissl, R., Kovács, A., Kreysa, E., Lanting, T. M., Lee, A. T., Lueker, M., Mehl, J., Menten, K. M., Muders, D., Nord, M., Plagge, T., Richards, P. L., Schilke, P., Schwan, D., Spieler, H., Weiss, A., & White, M. 2006, New Astronomy Review, 50, 960
Dunkley, J., Komatsu, E., Nolta, M. R., Spergel, D. N., Larson, D., Hinshaw, G., Page, L., Bennett, C. L., Gold, B., Jarosik, N., Weiland, J. L., Halpern, M., Hill, R. S., Kogut, A., Limon, M., Meyer, S. S., Tucker, G. S., Wollack, E., & Wright, E. L. 2009, ApJS, 180, 306
Dye, S., Ade, P. A. R., Bock, J. J., Chapin, E. L., Devlin, M. J., Dunlop, J. S., Eales, S. A., Griffin, M., Gundersen, J. O., Halpern, M., Hargrave, P. C., Hughes, D. H., Klein, J., Magnelli, B., Marsden, G., Mauskopf, P., Moncelsi, L., Netterfield, C. B., Olmi, L., Pascale, E., Patanchon, G., Rex, M., Scott, D., Semisch, C., Thomas, N., Truch, M. D. P., Tucker, C., Tucker, G. S., Viero, M. P., & Wiebe, D. V. 2009, ArXiv e-prints
Granato, G. L., De Zotti, G., Silva, L., Bressan, A., & Danese, L. 2004, ApJ, 600, 580
Greve, T. R., Ivison, R. J., Bertoldi, F., Stevens, J. A., Dunlop, J. S., Lutz, D., & Carilli, C. L. 2004, MNRAS, 354, 779
Güsten, R., Nyman, L. Å., Schilke, P., Menten, K., Cesarsky, C., & Booth, R. 2006, A&A, 454, L13
Halverson, N. W., Lanting, T., Ade, P. A. R., Basu, K., Bender, A. N., Benson, B. A., Bertoldi, F., Cho, H. ., Chon, G., Clarke, J., Dobbs, M., Ferrusca, D., Guesten, R., Holzapfel, W. L., Kovacs, A., Kennedy, J., Kermish, Z., Kneissl, R., Lee, A. T., Lueker, M., Mehl, J., Menten, K. M., Muders, D., Nord, M., Pacaud, F., Plagge, T., Reichardt, C., Richards, P. L., Schaaf, R., Schilke, P., Schuller, F., Schwan, D., Spieler, H., Tucker, C., Weiss, A., & Zahn, O. 2009, ApJ, 701, 42
Hill, R. S., Weiland, J. L., Odegard, N., Wollack, E., Hinshaw, G., Larson, D., Bennett, C. L., Halpern, M., Page, L., Dunkley, J., Gold, B., Jarosik, N., Kogut, A., Limon, M., Nolta, M. R., Spergel, D. N., Tucker, G. S., & Wright, E. L. 2009, ApJS, 180, 246
Hivon, E., Górski, K. M., Netterfield, C. B., Crill, B. P., Prunet, S., & Hansen, F. 2002, ApJ, 567, 2
Knox, L., Holder, G. P., & Church, S. E. 2004, ApJ, 612, 96
Komatsu, E., Dunkley, J., Nolta, M. R., Bennett, C. L., Gold, B., Hinshaw, G., Jarosik, N., Larson, D., Limon, M., Page, L., Spergel, D. N., Halpern, M., Hill, R. S., Kogut, A., Meyer, S. S., Tucker, G. S., Weiland, J. L., Wollack, E., & Wright, E. L. 2009, ApJS, 180, 330
Komatsu, E. & Seljak, U. 2002, MNRAS, 336, 1256
Muhleman, D. O. & Berge, G. L. 1991, Icarus, 92, 263
Negrello, M., Perrotta, F., González-Nuevo, J., Silva, L., de Zotti, G., Granato, G. L., Baccigalupi, C., & Danese, L. 2007, MNRAS, 377, 1557
Pacaud, F., Pierre, M., Adami, C., Altieri, B., Andreon, S., Chiappetti, L., Detal, A., Duc, P.-A., Galaz, G., Gueguen, A., Le Fèvre, J.-P., Hertling, G., Libbrecht, C., Melin, J.-B., Ponman, T. J., Quintana, H., Refregier, A., Sprimont, P.-G., Surdej, J., Valtchanov, I., Willis, J. P., Alloin, D., Birkinshaw, M., Bremer, M. N., Garcet, O., Jean, C., Jones, L. R., Le Fèvre, O., Maccagni, D., Mazure, A., Proust, D., Röttgering, H. J. A., & Trinchieri, G. 2007, MNRAS, 382, 1289

Pierre, M., Valtchanov, I., Altieri, B., & et al. 2004, Journal of Cosmology and Astro-Particle Physics, 9, 11
QUaD collaboration: R. B. Friedman, Ade, P., Bock, J., Bowden, M., Brown, M. L., Cahill, G., Castro, P. G., Church, S., Culverhouse, T., Ganga, K., Gear, W. K., Gupta, S., Hinderks, J., Kovac, J., Lange, A. E., Leitch, E., Melhuish, S. J., Memari, Y., Murphy, J. A., Orlando, A., O' Sullivan, C., Piccirillo, L., Pryke, C., Rajguru, N., Rusholme, B., Schwarz, R., Taylor, A. N., Thompson, K. L., Turner, A. H., Wu, E. Y. S., & Zemcov, M. 2009, ApJ, 700, L187
Reichardt, C. L., Ade, P. A. R., Bock, J. J., Bond, J. R., Brevik, J. A., Contaldi, C. R., Daub, M. D., Dempsey, J. T., Goldstein, J. H., Holzapfel, W. L., Kuo, C. L., Lange, A. E., Lueker, M., Newcomb, M., Peterson, J. B., Ruhl, J., Runyan, M. C., & Staniszewski, Z. 2009, ApJ, 694, 1200
Rudy, D. J., Muhleman, D. O., Berge, G. L., Jakosky, B. M., & Christensen, P. R. 1987, Icarus, 71, 159
Sayers, J., Golwala, S. R., Rossinot, P., Ade, P. A. R., Aguirre, J. E., Bock, J. J., Edgington, S. F., Glenn, J., Goldin, A., Haig, D., Lange, A. E., Laurent, G. T., Mauskopf, P. D., & Nguyen, H. T. 2009, ApJ, 690, 1597
Schwan, D., Bertoldi, F., Cho, S., Dobbs, M., Guesten, R., Halverson, N. W., Holzapfel, W. L., Kreysa, E., Lanting, T. M., Lee, A. T., Lueker, M., Mehl, J., Menten, K., Muders, D., Myers, M., Plagge, T., Raccanelli, A., Schilke, P., Richards, P. L. an d Spieler, H., & White, M. 2003, New Astronomy Review, 47, 933
Schwan, D. et al. 2009, in preparation
Sharp, M. K., Marrone, D. P., Carlstrom, J. E., Culverhouse, T., Greer, C., Hawkins, D., Hennessy, R., Joy, M., Lamb, J. W., Leitch, E. M., Loh, M., Miller, A., Mroczkowski, T., Muchovej, S., Pryke, C., & Woody, D. 2009, ArXiv e-prints; astro-ph/0901.4342
Shaw, L. D., Zahn, O., Holder, G. P., & Doré, O. 2009, ArXiv e-prints, astro-ph/0903.5322
Sievers, J. L., Mason, B. S., Weintraub, L., Achermann, C., Altamirano, P., Bond, J. R., Bronfman, L., Bustos, R., Contaldi, C., Dickinson, C., Jones, M. E., May, J., Myers, S. T., Oyarce, N., Padin, S., Pearson, T. J., Pospieszalski, M., Readhead, A. C. S., Reeves, R., Shepherd, M. C., Taylor, A. C., & Torres, S. 2009, ArXiv e-prints, astro-ph/0901.4540
Sunyaev, R. A. & Zel'dovich, Y. B. 1972, Comments on Astrophysics, 4, 173
Viero, M. P., Ade, P. A. R., Bock, J. J., Chapin, E. L., Devlin, M. J., Griffin, M., Gundersen, J. O., Halpern, M., Hargrave, P. C., Hughes, D. H., Klein, J., MacTavish, C. J., Marsden, G., Martin, P. G., Mauskopf, P., Moncelsi, L., Negrello, M., Netterfield, C. B., Olmi, L., Pascale, E., Patanchon, G., Rex, M., Scott, D., Semisch, C., Thomas, N., Truch, M. D. P., Tucker, C., Tucker, G. S., & Wiebe, D. V. 2009, ArXiv e-prints, astro-ph/0904.1200
Vikhlinin, A., Kravtsov, A. V., Burenin, R. A., Ebeling, H., Forman, W. R., Hornstrup, A., Jones, C., Murray, S. S., Nagai, D., Quintana, H., & Voevodkin, A. 2009, ApJ, 692, 1060
Willis, J. P., Pacaud, F., Valtchanov, I., Pierre, M., Ponman, T., Read, A., Andreon, S., Altieri, B., Quintana, H., Dos Santos, S., Birkinshaw, M., Bremer, M., Duc, P.-A., Galaz, G., Gosset, E., Jones, L., & Surdej, J. 2005, MNRAS, 363, 675
Zhang, Y.-Y., Böhringer, H., Finoguenov, A., Ikebe, Y., Matsushita, K., Schuecker, P., Guzzo, L., & Collins, C. A. 2006, A&A, 456, 55